Solid solution formation in $Mg_2(Si,Sn)$ and shape of the miscibility gap

M. Yasseri*[,a,b], A. Sankhla[b], H. Kamila[b], R. Orenstein[a,b,c], D.Y.N. Truong[b], N. Farahi[b], J. de Boor*[,b], E. Mueller[a,b]

[a]Institute of Inorganic and Analytical Chemistry, Justus Liebig University Giessen, D – 35392 Giessen, Germany.

[b]Institute of Materials Research, Linder Hoehe, German Aerospace Center (DLR), D – 51147 Koeln, Germany.

[c]Department of Materials Science and Engineering, Northwestern University, Evanston, IL 60208, USA.

*Corresponding Author(s): Mohammad.Yasseri@dlr.de, Johannes.deBoor@dlr.de

Abstract

Investigation of the thermochemical stability of $Mg_2(Si,Sn)$ thermoelectric materials is crucial for further development of thermoelectric modules. There is a miscibility gap reported for the quasibinary Mg_2Si–Mg_2Sn series, though the exact compositions of its limits are disputed. Gaining a better understanding of intersolubility limits in $Mg_2(Si,Sn)$ is important for further optimization of material performance by exploiting the gap-induced phase segregation. For a better understanding on the boundaries of the miscibility gap below 700 °C, two approaches were taken to provide evidence of thermodynamic stable phases and, hereby, monitor the borders of the miscibility gap. The approaches cover the homogenization of $Mg_2Si_xSn_{1-x}$ at 700 °C and diffusion couple experiments at 600 °C, 525 °C, and 450 °C. For 600 °C we find two ranges where Mg_2Si and Mg_2Sn are not miscible, namely $x = 0.35 \pm 0.05$ and $x = 0.75 \pm 0.05$ for miscibility gap I and $0.85 \pm 0.05 < x < 0.95 \pm 0.05$ for the second gap. The deduced complex

temperature dependence of the mixing / demixing behavior helps to understand the previously observed, apparently contradicting experimental results. We also show that there is no demixing for the compositions with the best thermoelectric properties at temperatures above 700 °C.

Keywords: Magnesium tin silicide, Thermoelectric, Miscibility gap, Solubility limit, Interdiffusion.

1 Introduction

$Mg_2Si_xSn_{1-x}$ solid solutions have attracted a lot of attention in recent years in the field of thermoelectric materials [1-5]. Light weight, environmental compatibility, abundance of constituent elements, and high thermoelectric performance (zT ~ 1.1 – 1.5) make these materials a potential candidate for waste heat recovery [1, 3]. Although some progress has been made in the development of Mg_2(Si,Sn) thermoelectric modules, only few studies are known on technological aspects of module development. Considering thermochemical stability of Mg_2(Si,Sn) at operational temperatures (450 °C – 500 °C) [6-10], thermodynamic and kinetic studies on the material system are crucial.

Desirably, a highly efficient thermoelectric material has a low thermal conductivity (κ) [11]. Nanostructuring in thermoelectric materials, e.g. by formation of multiphase morphology can lead to additional phonon scattering and, consequently, to a lower lattice thermal conductivity compared to single phase materials [12, 13].

A miscibility gap is reported in the pseudo-binary phase diagram of the Mg_2Si–Mg_2Sn material system, where a separation of the phases takes place [14, 15]. The reported gap is mapping of a temperature dependent solubility limits of Si and Sn in Sn-rich and Si-rich Mg_2(Si,Sn), respectively. A thermodynamically driven phase segregation caused by a miscibility gap opens a possibility for compositionally driven and high temperature-stable self-assembling of nanostructures by precipitation. Thus, understanding the intersolubility is crucial for a possible

further optimization of material performance. This strategy was followed, e.g., for PbTe based alloys like LAST-*m*: lead antimony silver telluride ($AgPb_mSbTe_{2+m}$) [16]. Phase segregation occurs for LAST-18 during quenching as a result of spinodal decomposition and nucleation, creating nanoinclusions of small size (~10 nm). This leads to overall vast enhancement of the figure of merit (zT) for LAST-18 compared to PbTe [16, 17].

The highest zT values for $Mg_2Si_xSn_{1-x}$ (zT = 1.1– 1.5) belong to the n-type compositions with a Si/Sn ratio between 30:70 and 40:60 [1-5]. However, it is not known whether those compositions are thermodynamically stable at the application temperatures (450 °C – 500 °C) [6-10]. It is clear that a possible phase separation in $Mg_2Si_xSn_{1-x}$ due to the miscibility gap is temperature dependent, though the reported results on the range of the miscibility gap are disputed and contradicting [14, 18]. Kozlov et al. have assessed the phase diagram of the $Mg_2Si_xSn_{1-x}$ system theoretically using CALPHAD and suggested the miscibility gap to cover the compositional range of $0.2 < x < 0.9$ at 600 °C [14]. The assessment of Kozlov et al. [14] was based on the experimental data had been previously obtained by Muntyanu et al. [19] using differential thermal analysis, microhardness measurements, specific gravity measurements, electrical conductivity and X-ray phase analyses. Nevertheless, Nikitin et al. [20] have conducted an experimental evaluation of the phase diagram and reported a different gap in the compositional range of $0.4 < x < 0.6$ at the same temperature. Their results were also based on X-ray and differential thermal analyses, microhardness and microstructure analyses, and density measurements [20]. Chen et al. synthesized Sb-doped $Mg_2Si_xSn_{1-x}$ samples with $0.2 < x < 0.9$ using a flux method followed by a hot pressing process at 700 °C – 840 °C and could obtain single phase $Mg_2Si_xSn_{1-x}$ solid solutions at any x within that range except for the compositions between $0.55 < x < 0.8$ [21]. They reported the latter compositional range as the miscibility gap at the pressing temperatures (700 °C – 840 °C) [21]. As their obtained miscibility gap differed from

the previously reported boundaries of the miscibility gap [14, 18-20], they suggested that the miscibility gap induced phase separation is related to Mg content (Mg excess and Mg vacancies) whose amount depends on synthesis method and parameters [21].

Sizov et al. [22] synthesized Si-rich $Mg_2Si_xSn_{1-x}$ samples and found a single phase material at 780 °C for x = 0.82, 0.87, 0.92, 0.94, and 0.97 which is in agreement with the solubility region reported in [21]. By annealing the samples at 680 °C and 580 °C for relatively long durations (1200 and 2400 min) they could observe phase separation [22]. Samples with compositions of x = 0.82 and 0.87 separated into Si-rich and Sn-rich compositions at 680 °C and 580 °C confirming existence of a miscibility gap at these temperatures.

Vives et al. [23] have carried out a set of diffusion couple experiments for the Mg_2Si–Mg_2Sn binary compounds and for the same temperature reported a gap in a range of $0.4 < x < 0.9$. However, no details on the related samples preparation procedures and their microstructure type were provided in the latter study [23]. Gorsse et al. [24] published another work based on the diffusion couple method reported in their previous work [23], proposing a layered structure, in which the composition and microstructural scaling vary from layer to layer aiming for a further reduction of the thermal conductivity in $Mg_2(Si,Sn)$. In that work induction melting was used for synthesis and Spark Plasma Sintering (SPS) was utilized to produce highly dense polycrystalline pellets [24]. Gorsse et al. [24] observed mainly six phases in their diffusion couple. Two of them were Si-rich $Mg_2Si_xSn_{1-x}$ ($x \simeq 0.9$ and $x \simeq 0.65$), one Sn-rich $Mg_2Si_xSn_{1-x}$ ($x \simeq 0.4$), one liquid phase surrounding one of the Si-rich compositions ($x \simeq 0.65$), and elemental Si and Sn, probably due to Mg loss. They reported that some melt-spun ribbons are formed due to rapid cooling which lead to a polymorphous solidification of the melt [24]. Gorsse et al. supposed that the $Mg_2Si_{0.65}Sn_{0.35}$ phase surrounded by the melt is a metastable supersaturated phase since its composition lies within their reported miscibility gap ($0.4 < x < 0.9$ at 600 °C) in Vives et al.

work [24]. Nevertheless, the complex microstructure might allow to question their reported intersolubility limits of Mg_2Si–Mg_2Sn from [23]. Also, no clear information is provided neither on the thermodynamic interplay of the liquid phase with $Mg_2Si_{0.65}Sn_{0.35}$ and other stable phases nor on the composition of the melt [24].

It is predicted by Niu et al. [25] and reported by Kozlov et al. [14] that there is a melt in equilibrium with the eutectic Mg_2Sn composition at temperatures higher than 560 °C, if the nominal composition is slightly richer than 66.66 at.% with Mg. The liquid phase is rich with Mg and contains e.g. ~ 90 mole % Mg at 560 °C [25].

Diffusion couples can be used to determine phase diagrams based on the assumption that there are local equilibria at the phase interfaces in the diffusion zone [26, 27]. Generally, due to the phase rule, in equilibrium, sharp interfaces with fixed compositional gaps develop which indicate a miscibility gap [26].

In a diffusion couple, the evolution of phases is based on solid state reactions [26]. However, if a liquid phase exists at the annealing temperature, the transport of matter is accelerated due to defects such as grain boundaries and cracks [26, 28, 29]. For instance if a pre-sintered rigid compact formed by solid state sintering is used as an end-member of a diffusion couple experiment, it can provide the possibility of capillary infiltration by an occurring liquid [30].

Therefore, to interpret diffusion couple experiments, we might need to consider the influence of a liquid phase, and a single diffusion model is not always adequate for the explanation of all results.

In this work we aimed for gaining a better understanding of the miscibility gap in the $Mg_2(Si,Sn)$ thermoelectric material system, through long term sintering and diffusion couple experiments. We found out that at 600°C there are two distinct immiscible regions with the limits being $x = 0.35 \pm 0.05$ and $x = 0.75 \pm 0.05$, and $0.85 \pm 0.05 < x < 0.95 \pm 0.05$. Furthermore, our results of

sintering experiments reveal an upper limit for the miscibility gap (< 700 °C) for the compositions with $x \leq 0.6$.

2 Experimental

$Mg_2Si_xSn_{1-x}$ samples were synthesized using commercially available starting elements (Mg turnings (Merck), Si (<6 mm, Chempur), and Sn (<71 μm, Merck) available with high purity >99.5%). A high-energy mechanical alloying mill (SPEX 8000D Shaker Mill) with stainless steel vials and balls was employed. The elements were weighed according to the desired stoichiometry ($Mg_2Si_xSn_{1-x}$ with x = 0, 0.4, 0.5, 0.6, 0.8, and 1). The ball milling was run mainly for 10-12 hours under argon to prevent oxidation and contamination. Powder samples were sintered in a graphite mold of Ø12.7 mm under vacuum (10^{-5} bar) using a sinter press (Direct Current Sintering Press DSP 510 SE) from Dr. Fritsch GmbH, Fellbach, Germany. Details on the synthesis of $Mg_2Si_xSn_{1-x}$ using high energy ball milling can be found in [2, 31]. $Mg_2Si_{0.5}Sn_{0.5}$ samples were sintered at 700 ˚C and 750 ˚C under 64 MPa with durations of 5, 20, 60, 120, and 300 min to investigate the stability of the Si-rich compositions in the compounds as well as the homogeneity of the samples (homogenization experiments). Moreover, $Mg_2Si_{0.4}Sn_{0.6}$ and $Mg_2Si_{0.6}Sn_{0.4}$ samples were sintered at 700 ˚C for 10, 20, and 60 min. $Mg_2Si_{0.8}Sn_{0.2}$ was sintered at 700 °C for 300 min. Mg_2Si and Mg_2Sn samples were sintered at 800 ˚C and 600 ˚C, respectively, for 10 min for the diffusion couple experiments. The density of the samples was measured using Archimedes' method. The relative densities of all the sintered samples were >95% of the theoretical value.

X-ray diffraction patterns were taken on powders and sample pellets utilizing a Siemens D5000 Bragg−Brentano diffractometer with a secondary monochromator, and a Bruker D8-advanced diffractometer with Cu Kα radiation (1.5406 Å) in the 2θ range 20−80° with a step size of 0.01°.

Diffusion couples were prepared by joining the Mg_2Si and Mg_2Sn pellets at 600 ˚C in the sinter press for 10, 300, and 600 min with direct current through the samples. For long term diffusion experiments, the diffusion couples (joint for 10 min) with additional elemental Mg were sealed in quartz ampules under argon (560 mbar) and magnesium vapor pressure to prevent oxidation, contamination, and Mg loss [32]. The samples were annealed at 450 ˚C, 525 ˚C, and 600 ˚C for approximately 6600 min.

Back scattered electron images were taken using a Zeiss Ultra 55 SEM with a Zeiss QBSE detector, also equipped with an Oxford energy dispersive X-ray (EDX) detector (PentaFETx3).

A quantification method introduced in our previous work [33] was used to determine the local composition and the (area) percentage with different compositional fractions in $Mg_2Si_xSn_{1-x}$ from backscattered electron image contrast. According to that method, knowledge of the grey value of the image pixels allows for a straightforward estimation of respective compositions (Si content) of different points of $Mg_2Si_xSn_{1-x}$ samples and quantification of areas with different compositions in BSE images.

3 Results

3.1 Homogenization Experiments

Details on the phase evolution of $Mg_2Si_xSn_{1-x}$ using high energy ball milling are discussed in [2]. An XRD pattern of the ball milled powder together with diffraction patterns of the $Mg_2Si_{0.5}Sn_{0.5}$ pellets sintered for different time durations are presented in Figure 1. The pattern of the $Mg_2Si_{0.5}Sn_{0.5}$ powder indicates that after ball milling for 12 hours (first step of the solid state reaction), some Sn-rich $Mg_2(Si,Sn)$ is formed while some amount of elemental Si and Mg remains unreacted in the multiphase material. The XRD pattern of the sample sintered at 700 °C for 5 min shows mainly $Mg_2Si_xSn_{1-x}$ peaks with some shouldering due to slight variations in *x*. The XRD patterns show no elemental impurities indicating complete consumption of the starting

elements as the solid state reaction is continuing during sintering. The XRD patterns of the samples sintered for 20 min and 60 min show that with increasing the sintering time at 700 °C (inset of Figure 1) the peaks become narrower (decrease in FWHM). There is a shoulder in the left side of the (220) peak of the sample sintered for 5 min, whereas the same peak for the samples sintered for 20 min and 60 min has no shoulder and is quite symmetrical. Also, there is a slight shift in all peaks positions towards lower 2θ (e.g. the (220) peak) for the samples sintered at 20 min and 60 min compared to the sample sintered at 5 min. The shoulder next to the (220) peak of the sample sintered for 5 min indicates that there are still some $Mg_2Si_xSn_{1-x}$ compositional inhomogeneities in the matrix, which are richer with Sn compared to the matrix after 5 min of sintering. The shoulder corresponding to the Sn-rich compositions vanishes for the samples sintered for longer durations since these Sn-rich inhomogeneities get dissolved into the matrix with time. This also explains the observed peak shift compared to the sample sintered for 5 min due to change in peak shape and the mean composition of the main peak. Furthermore, the XRD patterns of the samples sintered at 750 °C for 5 min and 20 min show that by increasing the sintering time, the separated Si-rich and Sn-rich peaks/phases existing after 5 min merged after 20 min. These trends indicate a homogenization of the local inhomogeneities remanent after milling in the $Mg_2Si_{0.5}Sn_{0.5}$ solid solution at 700 °C.

The results on the XRD patterns of $Mg_2Si_xSn_{1-x}$ samples with x=0.4, 0.5, and 0.6 sintered at 700°C for 60 min (Figure 1) indicate that (disregarding the minor MgO peak at 2θ (42°)), highly single phase pure (XRD-wise) samples of $Mg_2Si_xSn_{1-x}$ could be obtained, using the high energy ball milled powders. A gradual shift of the $Mg_2Si_xSn_{1-x}$ peaks toward higher 2θ (∼37°→ 39° for the 220 peak) with increasing the Si content (x) corresponds to a decreasing lattice parameter. The sample with x = 0.6 has a broader [220] peak compared to the other two compositions (x = 0.4 and x = 0.5) indicating a slower homogenization of the Si-rich samples compared to Sn-rich,

again in agreement with the finding from [2] that the Sn-rich solid solutions are formed faster than the Si-rich ones.

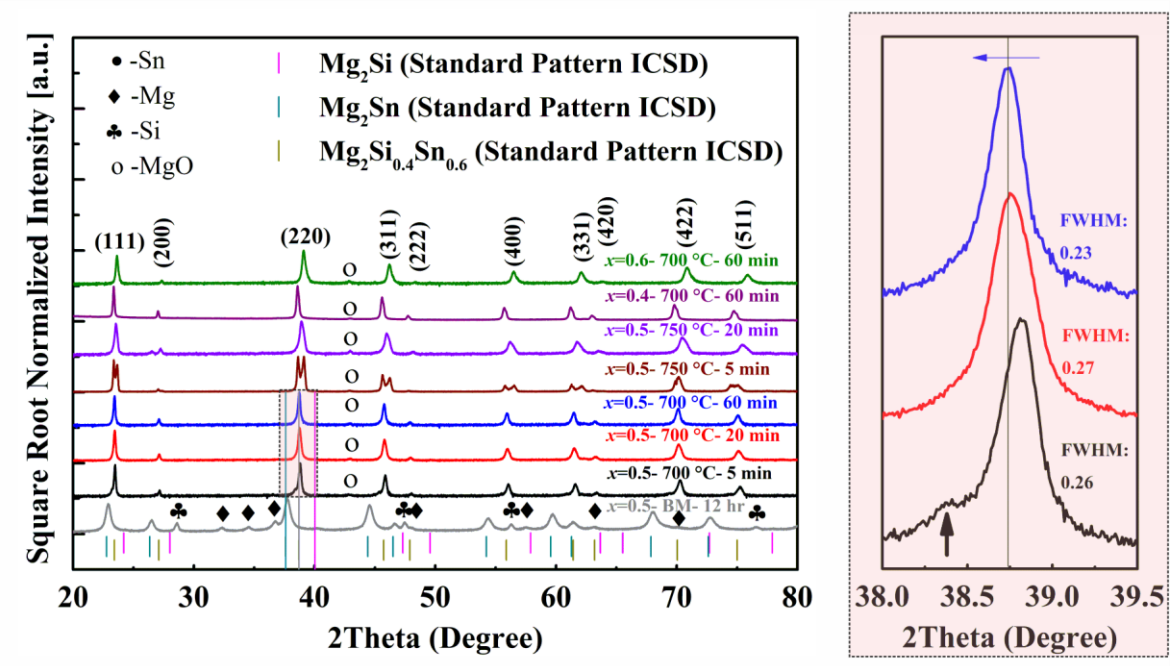

Figure 1: XRD patterns of $Mg_2Si_xSn_{1-x}$ samples with x = 0.4, 0.5, and 0.6 ball milled for 12 hours and sintered at 700 °C and 750 °C for 5, 20, and 60 min. The magnification (right) shows an enlarged view of the (220) peak (38°-39.5°) of the samples sintered at 700 °C for different time durations. The black arrow indicates a peak shoulder for the sample sintered for 5 min; blue arrow indicates a slight shift in the peak positions with longer sintering time.

Figure 2 (a - c) shows the SEM and EDX results (Point and ID overview) of the $Mg_2Si_{0.5}Sn_{0.5}$ samples ball-milled for 12 hours and sintered at 700 °C for different time durations of 20, 38, and 60 minutes. The point and ID overviews are plotted next to each image and show a variation of the compositions of the matrix as well as of the Si-rich regions as local inhomogeneities. Molar percentages of Si and Sn are mainly complementary for each point. The size of the Si-rich regions (darker regions) varies from less than 3 to 50 µm, with a median size of ~25 µm. The secondary phase regions have a concentric ring configuration with three levels of Si contents, namely, black, dark grayish (intermediate layer), and light grayish (matrix) areas for the sample

sintered for 20 min. The secondary phase regions get richer with Si towards the core. Remanent particles of elemental Si was found after extended ball milling previously [2]. We assume that the black Si-rich $Mg_2(Si,Sn)$ regions are the product of the reaction of remaining elemental Mg and elemental Si from ball-milling; with the Sn starting to substitute during the sintering step. The shape of the secondary regions changes gradually with time as they split into small, very Si-rich islands/grains, surrounded by areas with lower Si content (still above that of the matrix, though) as can be seen from the sample annealed for 38 min (Figure 2b, inset). The black islands (Si-rich) are probably corroded and dissolved by the dark grayish areas over time in a combination of slow bulk diffusion and stronger grain boundary diffusion. This results in a decoration of the grain structure of the material, hence, the appearance of the observed "cauliflower" structure. The ongoing dissolution is a consequence of diffusion driven homogenization following the completed solid state reaction. The amount of the secondary regions is minor for the sample sintered for 60 min (Figure 2c) even if the Si content still scatters in the darker regions.

The area percentage of the Si-rich regions which are surrounded by a matrix with a composition close to the nominal composition, corresponding to $x = 0.5$, can be quantified for all the samples using our recently developed quantification method based on the grey value of each pixel in the back scattered electron (BSE) images [33].

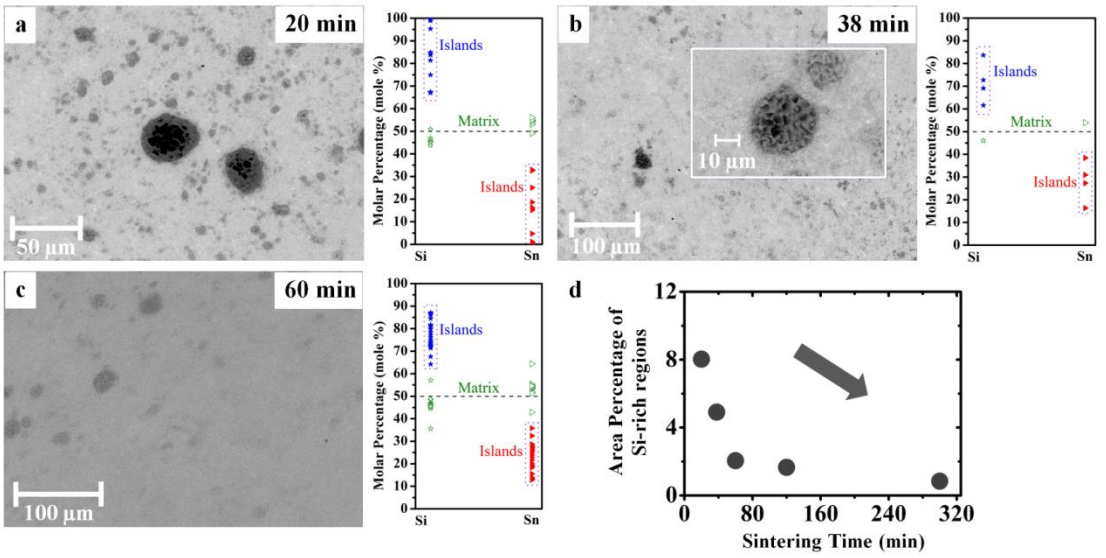

Figure 2: SEM and EDX results of the $Mg_2Si_{0.5}Sn_{0.5}$ samples annealed at 700 ˚C for 20 min (a), 38 min (with low and high magnifications) (b), and 60 min (c). The area percentage as obtained of the $Mg_2Si_xSn_{1-x}$ compositions with $x \geq 0.6$ in the $Mg_2Si_{0.5}Sn_{0.5}$ samples sintered at 700 ˚C for different time durations (20–300 min) is plotted in (d). The point and ID overviews of the samples are plotted next to each image and show variation of compositions in the matrix with $x = 0.48 \pm 0.02$ as well as the Si-rich regions.

The compositions with a Si deviation of $\Delta x \geq 0.1$ than the matrix composition (i.e. $x \geq 0.6$ for $Mg_2Si_{0.5}Sn_{0.5}$) is defined as Si-rich compositions in the $Mg_2Si_xSn_{1-x}$ solid solutions. The cumulative percentage of such compositions can be calculated for Si-rich regions as described in [33]. Figure 2d shows the area percentage of $Mg_2Si_xSn_{1-x}$ with $x \geq 0.6$ in the $Mg_2Si_{0.5}Sn_{0.5}$ samples sintered at 700 ˚C for different durations. Obviously, the area percentage of Si-rich compositions decreased with time at 700 ˚C, almost vanishing after 300 min. This result confirms the XRD results (Figure 1) indicating the dissolution of the Si-rich solid solution into the matrix and implying the homogenization of the samples with the sintering time.

The area percentage of the Si-rich regions in the $Mg_2Si_{0.6}Sn_{0.4}$, $Mg_2Si_{0.4}Sn_{0.6}$, and $Mg_2Si_{0.8}Sn_{0.2}$ samples is given in Table 1. The area percentage of the Si-rich regions is minor after sintering

and decreases with increasing sintering time at 700 ˚C. These results confirm the trend of homogenization ending up with a single phase of $Mg_2Si_xSn_{1-x}$ at 700 ˚C for all starting compositions. We also observed in the region of x = 0.4 to 0.6 that the amount of secondary phases increases with an increase in the Si content (x), in agreement with the broadening of the XRD peaks for $Mg_2Si_xSn_{1-x}$ with increasing x (Figure 1).

Table 1: Area percentages of the Si-rich regions ($\Delta x \geq 0.1$) in the $Mg_2Si_xSn_{1-x}$ compositions. SEM images corresponding to the $Mg_2Si_{0.8}Sn_{0.2}$ samples can be found in the supporting information (Figure S1).

Matrix Composition	Area Percentage (%) (with Sintering Time 1)	Area Percentage (%) (with Sintering Time 2)
x = 0.4	2 % (5 min)	1 % (20 min)
x = 0.5	11 % (20 min)	2 % (60 min)
x = 0.6	-	4 % (60 min)
x = 0.8	0.17 % (60 min)	0 % (300 min)

All in all, the results imply that for any of the studied initial stoichiometries, Si-rich and Sn-rich regions get dissolved into each other at 700 °C as the XRD peaks merge (Figure 1). From Figure 2 can be read that no miscibility gap exists between x = 0.5 and about x = 0.65 at temperatures higher than 700 °C. This conclusion is in agreement with results reported on the synthesis of $Mg_2Si_{0.5}Sn_{0.5}$, where a single phase material had been obtained at synthesis temperatures of 700 °C – 800 °C [34-36].

The compositional map of Figure 2a is plotted in the supporting information (Figure S2). There are two gaps in the counts of the $Mg_2Si_xSn_{1-x}$ compositions for the sample annealed at 700 °C for 20 min. This as well as the observation of two sharp changes in composition surrounding the Si-

rich $Mg_2(Si,Sn)$ inclusions in Figure 2 hints at the existence of two narrow gaps which persist at this temperature, one below and one above $x = 0.8$.

3.2 Diffusion Couple Experiments

After obtaining pure Mg_2Sn and Mg_2Si samples which were polycrystalline with a grain size of 1–10 µm, diffusion couple experiments were carried out (corresponding XRD and SEM results are shown in Figure S2 and Figure S4).

Figure 3a shows the interface of a Mg_2Si–Mg_2Sn diffusion couple joint at 600 °C for 300 min in a sinter press.

Unlike observations as reported by Vives et al. [23] where continuous concentration profiles were obtained at both sides of the interface of a diffusion couple, our micrograph shows several features which cannot be explained by a simple one-dimensional diffusion model. Several striking discontinuities are found in the local concentration distribution which can be understood assuming material transport by melt infiltration additionally to homogenization by diffusion, rapid grain boundary diffusion coacting with slower bulk diffusion as well as the occurrence of gaps in the intersolubility of the $Mg_2(Si,Sn)$ solid solutions series.

There is for instance a light grey bulged region right at the interface of Mg_2Si and Mg_2Sn (indicated with a black arrow). The bulged region has a wavy microstructure and is not formed as a coherent layer along the Mg_2Si–Mg_2Sn interface. Also, there are some regions between the Mg_2Si grains close to the interface of the diffusion couple which are brighter (have lower grey values) than the matrix. Figure 3c shows a zoomed view of the Sn-rich side of a diffusion couple pressed for 600 min at 600 °C. There, we observe some nano-sized whitish round spheres (indicated by black circles). Figure 3d shows the Mg_2Si side of the couple. The morphology resembles a solid-liquid phase situation. Obviously, a melt has wetted and partially dissolved Mg_2Si particles (grains) which probably has entered the Mg_2Si side by infiltration along the grain

boundaries and coexisted together with $Mg_2(Si,Sn)$ phases at 600 °C for hours. According to the phase diagram of the binary Mg-Sn system, a liquid phase is existing below 600 °C with a composition close to $Mg_{0.9}Sn_{0.1}$ [25] whereas no liquid phase occurs at this temperature in the Mg-Si system [37]. We believe that the nano-sized whitish spheres in Mg_2Sn (Figure. 3c) are left-overs of small Mg-Sn melt inclusions which have been formed as the material synthesis involved overstoichiometric Mg. In this work, Mg_2Sn samples were prepared by 7.5 mole% excess Mg, intending to compensate the Mg loss that is accompanying $Mg_2(Si,Sn)$ synthesis at elevated temperatures [10, 38, 39]. Obviously, elemental Mg has remained after compaction in the Sn-rich side of the diffusion couple. In contact to Mg_2Sn, elemental Mg dissolves some of it at 600 °C to form a Mg-Sn melt. Under pressure at 600 °C, some of the melt droplets were presumably squeezed out of the Sn-rich side. The melt accumulated at particle interfaces and at the interface of the Mg_2Si–Mg_2Sn diffusion couple forming wavy microstructures as the observed one and infiltrated along the grain boundaries into the Mg_2Si side followed by slow homogenization of the Mg-Sn melt with Mg_2Si into Sn-enriched $Mg_2(Si,Sn)$ which will be discussed later. Also, using our BSE quantification method [33], we deduce from the grey values of the brighter regions on the Mg_2Si side in Figure 3a that these regions are $Mg_2(Si,Sn)$ but formed from the Mg_2Si matrix by interdiffusion of Sn, Si and Mg. The grain boundaries of the Si-rich side are decorated by Mg and Sn, infiltrated as a melt. In Figure 3a, it is also seen that diffusion carries Sn into grains at the Mg_2Si side, most of them close to the Mg_2Si–Mg_2Sn interface of the diffusion couple but some also farther away. The compositional map of Figure 3a is plotted in Figure 3b. The compositions of $Mg_2Si_xSn_{1-x}$ at the interface are around $x = 0.75 \pm 0.05$ and $x = 0.35 \pm 0.05$ in the grains at the Si-rich and Sn-rich sides, respectively.

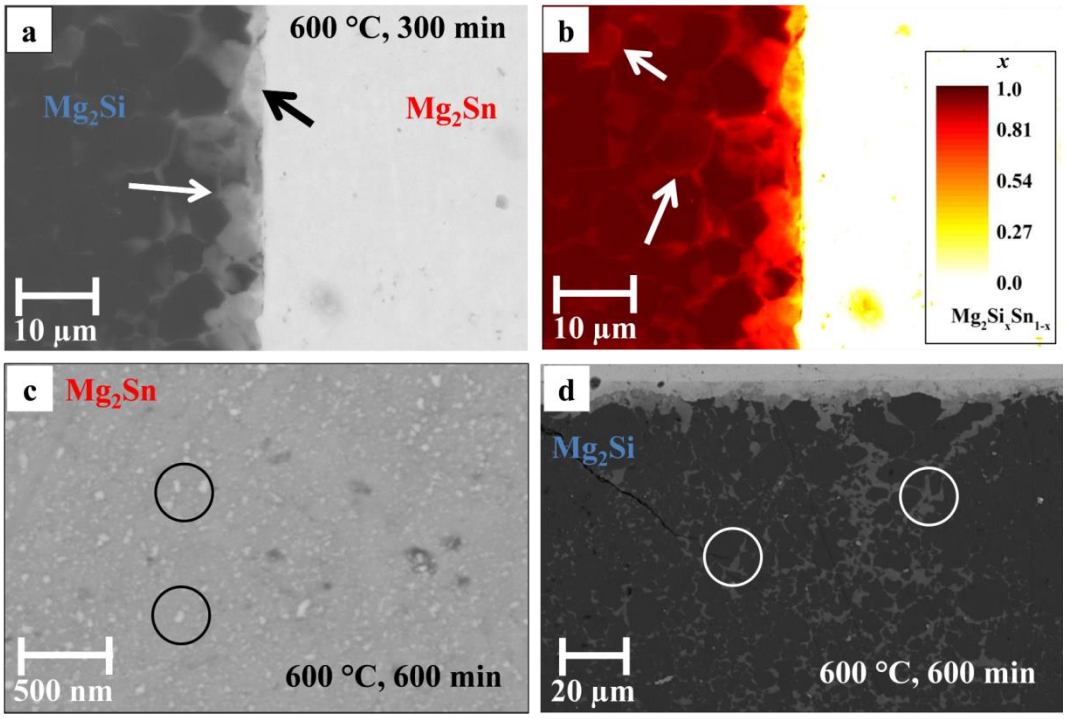

Figure 3: BSE image (a) and its corresponding quantification map (b) of the diffusion couple pressed at 600 °C for 300 min. The black arrow indicates an area where Mg-Sn melt has first accumulated at the interface and later converted into $Mg_2(Si,Sn)$. The white arrow in (a) shows grains where Sn has diffused into Mg_2Si crystallites replacing Si. The compositions of the crystallites at the yellow-to-red interface are around $x = 0.75 \pm 0.05$ and $x = 0.35 \pm 0.05$ at the Si-rich and Sn-rich sides of the diffusion couple, respectively. White arrows in (b) indicate the infiltration of Mg-Sn into Mg_2Si and its dissolution into the grains starting from the grain boundaries. Figure (c) and (d) show the Mg_2Sn and Mg_2Si sides of the diffusion couple pressed at 600 °C for 600 min, respectively. Black circles indicate nano-sized solidified Mg-Sn melt in the Sn-rich side and white arrows show infiltration of the melt along the grain boundaries of Mg_2Si.

At the same time with the thermal treatment, Mg evaporates continuously from the system [24, 32], depleting the melt in the Mg content, turning it into Mg_2Sn again. By XRD on the cross section of the Mg_2Si–Mg_2Sn diffusion couples joint at 600 °C for 300 min and annealed at 600 °C for 6600 min, we could observe an indication of Mg loss. The corresponding results are shown in Figure S6. In the XRD pattern of the sample annealed for 6600 min, there are some peaks corresponding to elemental Sn whereas no elemental Sn was recognized in the XRD pattern of the diffusion couple joint at 600 °C for 300 min before this temperature treatment.

Also, there was no peak of elemental Sn in the XRD pattern of the Mg_2Sn member before the joining and annealing steps (Figure S2). It indicates that some elemental Sn precipitated with time in the diffusion couple while annealing at 600 °C. We believe that the precipitation of the elemental Sn in the sample is due to the Mg loss with time as a result of the limited solubility of overstoichiometric *X* (Si, Sn) component in Mg_2X.

However, the transport of matter over the Mg_2Si–Mg_2Sn interface does not look symmetrically at all. In contrast to the clearly identified invasion of Sn into the Mg_2Si rich side by diffusion and infiltration, the diffusion of Si into the Mg_2Sn side seems quite slow; hardly any evidence of a diffusion margin of Si decaying into the depth of the Mg_2Sn side after 300 min at 600 °C can be read from Figure 3.

Figure 4 shows a BSE image together with its corresponding compositional map of a Mg_2Si–Mg_2Sn diffusion couple annealed at 600 °C for 6600 min. The compositions of $Mg_2Si_xSn_{1-x}$ in the regions adjacent to the interface are around $x = 0.75 \pm 0.05$ and $x = 0.35 \pm 0.05$ at the Si-rich and Sn-rich sides, respectively. The diffusion margin of Si at the Mg_2Sn side which was hardly identifiable after 300 min is now clearly seen and comparably wide as on the other side. Possibly, Si-Sn interdiffusion is weak in Mg_2Sn saturated with Mg but increases with ongoing Mg depletion. There are also some grains similar to isolated islands in the distance of 100 µm from the interface at the Si-rich side that have only little Sn content (indicated by blue circles in Figure 4a). Similarly as for Mg_2Sn, we can assume that also Mg_2Si is stabilized by Mg saturation against Si-Sn interdiffusion. An Mg_2Si particle surrounded by Mg-Sn melt although slowly dissolved at its free surfaces (limited by the solubility of Si in the melt) would thus be kept for a longer time at its original composition until the melt is depleted in Mg when it starts to interdiffuse faster. The histogram with respect to the Si:Sn composition for the image (Figure 4b) shows a clear

decrease in counts for $0.35 < x < 0.75$ and a second minimum for $0.85 < x < 0.95$ pointing to the occurrence of not just one but two miscibility / intersolubility gaps (blue bars).

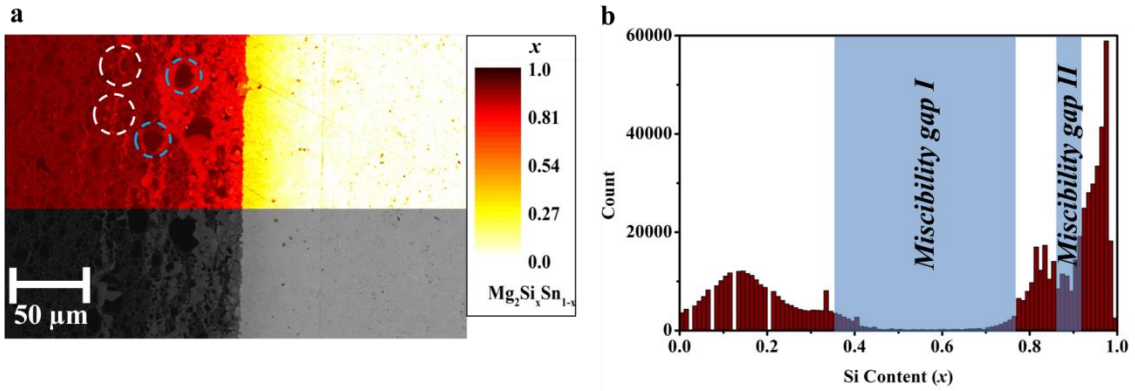

Figure 4: (a) BSE image (bottom) and its corresponding compositional map (above) of the diffusion couple annealed at 600 °C for 6600 min. The compositions of the crystallites at the yellow-to-red interface are around $x = 0.75 \pm 0.05$ and $x = 0.35 \pm 0.05$ for $Mg_2Si_xSn_{1-x}$ at the Si-rich and Sn-rich sides of the diffusion couple, respectively. Sn enrichment due to Mg-Sn melt infiltration around the grains at the Si-rich side is indicated by white dashed circles (a). Blue dashed circles indicate Mg_2Si grains with low Sn content. Counts of pixels with their respective compositions are plotted in (b).

The Mg-Sn melt infiltrated along the grain boundaries of Mg_2Si grains within a distance of 500 µm from the interface (examples indicated by dashed white circles in Figure 4a). The grain boundaries act as transport channels for the Mg-Sn melt and, as a consequence, as sources of Sn atoms for diffusion into Mg_2Si grains. We also observe that, qualitatively similar to the situation after 300 min of annealing (Figure 3), the change in composition from the Mg_2Sn side towards the junction is quite smooth while the Mg_2Si side has striking discontinuities in the composition. The difference is due to a mainly diffusion controlled transport of Si into Mg_2Sn whereas in the Mg_2Si side the Mg-Sn melt infiltration is dominant. The melt infiltration occurred probably instantaneously at the beginning of the joining step in the hot press followed by diffusion processes where the Sn source is not only the initial Mg_2Si–Mg_2Sn flat interface, but also Sn deposits in cracks and grain boundaries formed by the infiltration structure. The Sn-rich channels penetrating the Mg_2Si side act as short-cuts for diffusion of Sn into Mg_2Si grains leading to a

quite inhomogeneous compositional gradient from the junction towards the Mg_2Si side. On the Mg_2Sn side, Si atoms diffused mainly into the Mg_2Sn bulk within a diffusion zone width of about 50 µm. There is no hint on Si moving preferentially along grain boundaries of Mg_2Sn crystallites. Si atoms move from Mg_2Si over the interface and into the infiltrated melt where they, to a low degree, may dissolve. The melt is acting as a flux allowing Mg_2Sn to dissolve or crystallize from it, forming smooth and round droplet morphologies. Due to the limited solubility of Si in the melt the exchange of matter between the melt and Mg_2Si is much weaker than that between the melt and Mg_2Sn. The exchange of matter of the melt droplets with $Mg_2(Si,Sn)$ is also limited as it can proceed only assisted by solid state interdiffusion of Si and Sn, by the low variability of the Mg:*X* ratio in $Mg_2(Si,Sn)$. Likewise, diffusion of Si into Mg_2Sn, by the low variability of the Mg:*X* ratio, is closely interlinked to counter-directed Sn diffusion or simultaneous Mg diffusion, forming $Mg_2(Si,Sn)$ solid solutions at both sides of the diffusion interface. The compositions of the solid solutions formed at both sides of the interface are limited by finite solubility of Si in Mg_2Sn and Sn in Mg_2Si, respectively.

The isolated dark islands (blue encircled) on the Si-rich side of the Figure 4a indicate a second miscibility / intersolubility gap present in the material system. The small gap in Figure 4b indicates the boundaries of the second miscibility gap. The second miscibility gap opens between $x = 0.85 \pm 0.05$ and $x = 0.95 \pm 0.05$. The results remind on the work of Gorsse et al. [24], where two types of Si-rich compositions were found together with Sn-rich $Mg_2Si_xSn_{1-x}$. There, one Si-rich phase was supposedly at the boundary of the reported miscibility gap ($x \simeq 0.9$) [23, 24]. The second Si-rich composition ($x = 0.65$) was supposed to be metastable since it lies within the boundaries of the miscibility gap at 600 °C [24]. We think it is misunderstood and these two Si-rich phases in Gorsse et al. [24] had been the Si-rich boundaries of the two solubility / miscibility gaps.

Figure 5 shows the BSE image of the sample annealed at 600 °C for 6600 min and an EDX line scan where the data from 14 parallel line scans has been accumulated numerically. We observe a gradual increase in the Si content from right to left (from the Mg_2Sn end towards the junction). There is a jump in the composition from around Si ~ 12 at. % ($x \simeq 0.36$) to ~ 26 at. % ($x \simeq 0.78$) at the interface. After an abrupt jump in the Si content at the junction, there is again an increase in the Si content within a zone with the Mg_2Si crystallites towards the end. This corresponds to solubility limits of Sn in Mg_2Si and Si in the Mg_2Sn for the (larger) miscibility gap I of ~ 8 ($x \simeq 0.76$) and ~12 atomic % ($x \simeq 0.36$), respectively, as indicated by the dashed lines. We furthermore observe a fluctuation of the Si content on the Si-rich side, while on the Sn-rich side the curve is quite smooth. Presumably, the Si content does not change monotonously with distance because on the Si-rich side we have an interplay between fast Mg-Sn melt infiltration and slower crystallite diffusion. The fluctuations in the compositions can also give an indication of presence of the second miscibility gap (see around 75 µm), where the Si contents fluctuate between the compositions responsible for the boundaries of the second miscibility gap.

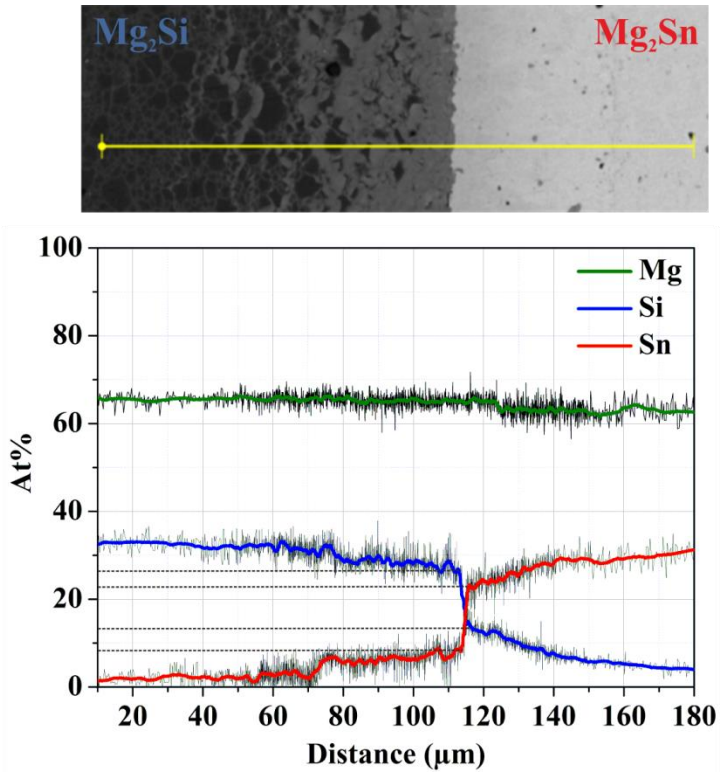

Figure 5: BSE image and its corresponding EDX line scans of the diffusion couple annealed at 600 °C for 6600 min. The black lines are obtained by numerical accumulations of 14 parallel line scans across the diffusion interface and the colored lines are obtained after smoothing the black lines. The dashed lines indicate the steps in the Si and Sn contents at the diffusion interface.

4 Discussions

Mg_2Si–Mg_2Sn diffusion couple experiments reveal a rich and complex microstructure that cannot be explained by solid state diffusion only. Instead we argue that it can be explained by a combination of a Mg-Sn melt infiltration and solid state interdiffusion. Compositional analysis shows that at 600 °C we have two distinct immiscible regions with the limits being $x = 0.35 \pm 0.05$ and $x = 0.75 \pm 0.05$ for miscibility gap I and $0.85 \pm 0.05 < x < 0.95 \pm 0.05$ for miscibility gap II. The existence of two miscibility gaps is also in agreement with the homogenization experiments at 700 °C. The existence of a miscibility gap region with a narrow compositional range in the Si-rich side of the pseudo-binary Mg_2Si–Mg_2Sn at temperatures higher than 700 °C was also reported previously by Chen et al. [21], where they observed a miscibility gap region in

a compositional range of $0.55 < x < 0.8$ at 700 °C – 840 °C. Though Chen et al. [21] did not obtain the boundaries of the miscibility gap at a very same temperature and their homogenization temperatures vary between 700 °C – 840 °C, we think the miscibility gap region found by Chen et al. is in agreement with our first miscibility gap (miscibility gap I) which got narrow at 700 °C. As they suggested, the differences in the Mg content might be the reason of the difference between the first gap estimated in our study (miscibility gap I at 700 °C: $0.65 < x < 0.75$) and what they reported [21]. It should be noted that they did not investigate compositions with $x > 0.9$ which can be the reason why they could not discover the miscibility gap II ($0.85 \pm 0.05 < x < 0.95 \pm 0.05$). Also, Sizov et al. [22] had observed two Si-rich phases existing in some of the samples with the nominal compositions of $x = 0.92$, 0.94, and 0.97 annealed at 580 °C and 680 °C. Though according to [22] these phases are possibly formed through spinodal decomposition while cooling down and had varying compositions (e.g. $x_1 = 0.911$, 0.977, and 0.987 and $x_2 = 0.926$ and 0.944 at 680 °C), we think the co-existence of two Si-rich phases might also be a confirmation for the existence of the miscibility gap II in the Si-rich side of the phase diagram at temperatures higher than 580 °C, as no Sn-rich phase was observed in the case of samples with two separated Si-rich phases [22]. The existence of miscibility gap with a complex temperature dependence is unusual but has already been observed in mixed crystals such as Au-Pt [40], Au-Cu [40], and Fe-Cr [41]. A two-peak miscibility gap is formed when the magnitude of the positive enthalpy of mixing is slightly lowered in the intermediate composition range [42].

It should be noted that the atomic percentage at the concentration spikes corresponding to the immiscibility range does not vary with time (compare 300 min (Figure 3a and 3b), and 6600 min (Figure 4 and 5)) proving that further factors which might shift solubility limits (as, possibly Mg:*X*) did not change during the long annealing as much as to significantly shift the limits. We believe the results reported by Vives et al. [23] as the solubility limits of Sn in Mg_2Si and Si in

the Mg_2Sn ($x \simeq 0.45$ and $x \simeq 0.93$ at 600 °C) are the Sn-rich boundary of our miscibility gap I and Si-rich boundary of the miscibility gap II. Therefore, our results agree well with the literature data, where a diffusion couple technique was used [23].

The solubility limits of $x \simeq 0.30$ and $x \simeq 0.27$ for Si in Mg_2Sn are obtained by means of diffusion couple experiments at 525 °C and 450 °C, respectively (see supplementary materials, Figure S5-a and Figure S5-b). For these experiments we do not observe indications for melt infiltration in agreement with being below the lowest melting temperature in the Mg-Sn system. Furthermore we do not find hints for the existence of two distinct immiscible regions, in difference to the results at 600°C. Considering the limited spatial resolution of EDX and the very close solubility limits of Si in Mg_2Sn at 525 °C and 450 °C, the boundary of the miscibility gap in the Sn-rich side of the pseudo-binary phase diagram cannot be reported more precise than $x = 0.3 \pm 0.1$ for both of the temperatures (525 °C and 450 °C). The compositions corresponding to the obtained Si solubility limits in Mg_2Sn at 525 °C and 450 °C are in vicinity of some of the Sn-rich compositions formed after phase separation due to the miscibility gap at 580 °C in [22]. The increase in the demixing width at the lower temperatures is in agreement with the theoretical calculations by the CALPHAD [14, 18] and DFT [15] methods, where the mixing energy for Mg_2Si-Mg_2Sn is always positive (unfavorable) which is compensated by an entropy term that becomes larger with increasing temperature.

Figure 6 shows the obtained boundaries of the miscibility gap (in a temperature range of 450 °C – 600 °C) from our diffusion couple and sintering experiments (at 700 °C) together with the reported results in literature. Furthermore, our results of sintering experiments reveal an upper limit for the miscibility gap (< 700 °C) for the compositions around $x \simeq 0.4$ which have the best thermoelectric properties. The difference in the results on the miscibility gap with previous works [14, 15, 18] might be due to improvements in the quality of preparation and chemical analysis

facilities (SPS, DSP, and EDX, and WDX) in recent decades. The improvement in the preparation and measurement facilities lead to e.g. a more successful avoidance of Mg evaporation [10, 32] as well as a better spatial resolution of scanning electron microscopes, therefore more exact results for the miscibility range.

We also found the miscibility gap to be asymmetrical, which is in agreement with the calculations of Viennois et al. [15]. Furthermore, the obtained results are in agreement with calculations considering the increase in the width of miscibility gap with decreasing the temperature [14, 15, 18]. However, it seems that in the theoretical works, the effect of the temperature on the demixing behavior is overestimated as the miscibility ranges obtained from the experimental works are all narrower than the results from the calculations.

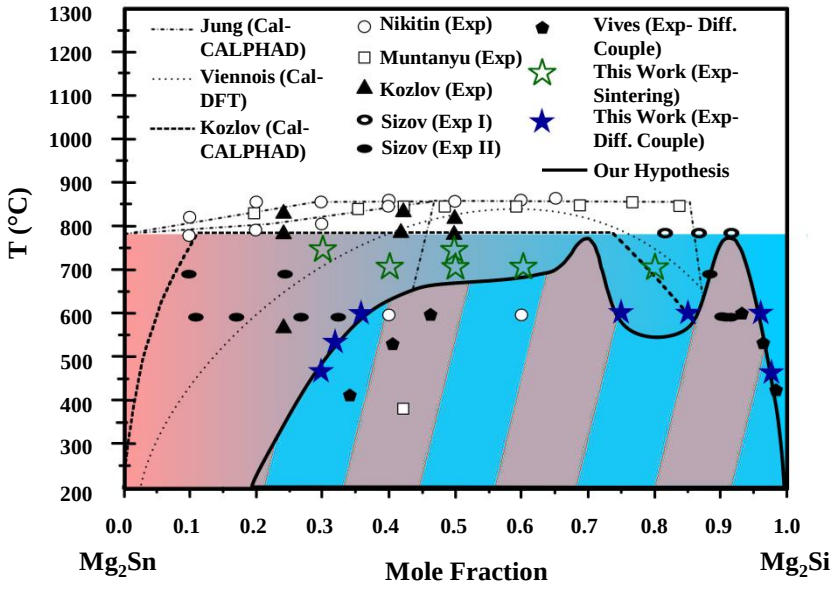

Figure 6: The obtained miscibility gap in this study together with different reports on the miscibility gap in literature [14, 15, 18-20, 23]. Nikitin et al. [20] and Muntyanu et al. [19] had carried out XRD, thermal analysis, microhardness measurements, and density measurements to obtain boundaries of the miscibility gap. Also, Kozlov et al. [14] had obtained their experimental data by differential scanning calorimetry and thermal analysis. Sizov et al. [22] had conducted sintering experiments (Exp I) and obtained Si-rich single phase solid solutions (empty ovals). The solid solutions were then annealed at lower temperatures (Exp II) which then underwent phase separation to form Si-rich and Sn-rich phases (filled ovals) [22]. Empty stars indicate our experimental data

with $Mg_2(Si,Sn)$ compositions at which formation of a homogenous solid solution was proven. Filled stars with blue show our experimental data indicating the solubility limits (boundaries of the miscibility gap at 450 – 600 °C). The solid black line is plotted as a guide to the eye to indicate our hypothesis for the position of the miscibility gap.

We note that a dependence of the limits of the miscibility gap on the strain in the materials has recently been predicted [43]. We did not observe a difference between results from experiments obtained under pressure (sintering) or pressureless (diffusion couples). However, the stress applied in our experiments is much smaller than the stress theoretically required for a visible difference.

5 Conclusions

In this study we investigated the boundaries of the miscibility gap of the pseudo-binary phase diagram of the Mg_2Si–Mg_2Sn quasi-binary material system. Sintering and diffusion couple experiments reveal a rich microstructure, from the analysis of which we conclude i) the existence of a Mg-Sn melt at 600°C which results in an altered material transport compared to solid state diffusion and ii) a complex temperature dependence of the miscibility gap leading to two immiscible regions at 600 °C. For the compositions with the best thermoelectric properties ($Mg_2Si_{0.5}Sn_{0.5}$ - $Mg_2Si_{0.3}Sn_{0.7}$) we prove a complete solubility below 700 °C. This unravels the apparent contradiction between previously reported single phase samples of $Mg_2Si_{0.5}Sn_{0.5}$ [34-36] and the fact that $Mg_2Si_{0.5}Sn_{0.5}$ is reported to be within the miscibility gap in basically all reports [14, 15, 18-20, 23, 43]. The discovery of a second miscibility gap furthermore explains some of the inconsistencies in previous reports. A more accurate description of the homogenization and demixing behavior in the Mg_2Si–Mg_2Sn system will allow for a tailoring of the structural features of the material and hence a further optimization of the thermoelectric properties.

Acknowledgments

The authors would like to gratefully acknowledge the endorsement from the DLR Executive Board Member for Space Research and Technology and the financial support from the Young Research Group Leader Program. M.Y. and R.O. would like to thank for their financial support which is provided by the DFG via the GRK (Research Training Group) 2204 "Substitute Materials for Sustainable Energy Technologies“. Financial supports of A. S., H. K., D.Y.N.T., and N. F., are provided by the DAAD fellowship. Also, R.O. would like to acknowledge the DAAD-RISE program for her summer internship opportunity. The authors would like to thank to G. Castillo-Hernandez and P. Ponnusamy (DLR) for their support with the data handling.

Appendix A. Supplementary data

Supplementary data related to this article can be found at http:// dx.doi.org/xxx.

References

[1] N. Farahi, S. Prabhudev, G.A. Botton, J.R. Salvador, H. Kleinke, Nano- and Microstructure Engineering: An Effective Method for Creating High Efficiency Magnesium Silicide Based Thermoelectrics, ACS Appl Mater Interfaces 8(50) (2016) 34431-34437.
[2] A. Sankhla, A. Patil, H. Kamila, M. Yasseri, N. Farahi, E. Mueller, J. de Boor, Mechanical Alloying of Optimized Mg2(Si,Sn) Solid Solutions: Understanding Phase Evolution and Tuning Synthesis Parameters for Thermoelectric Applications, ACS Applied Energy Materials 1(2) (2018) 531-542.
[3] V.K. Zaitsev, M.I. Fedorov, E.A. Gurieva, I.S. Eremin, P.P. Konstantinov, A.Y. Samunin, M.V. Vedernikov, Highly effectiveMg2Si1−xSnxthermoelectrics, Physical Review B 74(4) (2006).
[4] J. de Boor, T. Dasgupta, U. Saparamadu, E. Müller, Z.F. Ren, Recent progress in p-type thermoelectric magnesium silicide based solid solutions, Materials Today Energy 4 (2017) 105-121.
[5] W. Liu, X. Tan, K. Yin, H. Liu, X. Tang, J. Shi, Q. Zhang, C. Uher, Convergence of conduction bands as a means of enhancing thermoelectric performance of n-type Mg2Si(1-x)Sn(x) solid solutions, Phys. Rev. Lett. 108(16) (2012) 166601.
[6] G. Skomedal, N.R. Kristiansen, M. Engvoll, H. Middleton, Methods for enhancing the thermal durability of high-temperature thermoelectric materials, J. Electron. Mater. 43(6) (2014) 1946-1951.
[7] G. Skomedal, L. Holmgren, H. Middleton, I. Eremin, G. Isachenko, M. Jaegle, K. Tarantik, N. Vlachos, M. Manoli, T. Kyratsi, Design, assembly and characterization of silicide-based thermoelectric modules, Energy Convers. Manage. 110 (2016) 13-21.
[8] J. de Boor, D. Droste, C. Schneider, J. Janek, E. Mueller, Thermal Stability of Magnesium Silicide/Nickel Contacts, J. Electron. Mater. 45(10) (2016) 5313-5320.
[9] N.H. Pham, N. Farahi, H. Kamila, A. Sankhla, S. Ayachi, E. Müller, J. de Boor, Ni and Ag electrodes for magnesium silicide based thermoelectric generators, Materials Today Energy 11 (2019) 97-105.
[10] G.K. Goyal, T. Dasgupta, Effect of Magnesium Content and Processing Conditions on Phase Formation and Stability in Mg2+δSi0.3Sn0.7, J. Electron. Mater. 47(3) (2018) 2066-2072.
[11] G.J. Snyder, E.S. Toberer, Complex thermoelectric materials, Nat Mater 7(2) (2008) 105-14.

[12] A. Yamini, T. Li, D.R.G. Mitchell, J.M. Cairney, Elemental distributions within multiphase quaternary Pb chalcogenide thermoelectric materials determined through three-dimensional atom probe tomography, Nano Energy 26 (2016) 157-163.
[13] L.-D. Zhao, V.P. Dravid, M.G. Kanatzidis, The panoscopic approach to high performance thermoelectrics, Energy Environ. Sci. 7(1) (2014) 251-268.
[14] A. Kozlov, J. Gröbner, R. Schmid-Fetzer, Phase formation in Mg–Sn–Si and Mg–Sn–Si–Ca alloys, J. Alloys Compd. 509(7) (2011) 3326-3337.
[15] R. Viennois, C. Colinet, P. Jund, J.-C. Tédenac, Phase stability of ternary antifluorite type compounds in the quasi-binary systems Mg2X–Mg2Y (X, Y = Si, Ge, Sn) via ab-initio calculations, Intermetallics 31 (2012) 145-151.
[16] M.G. Kanatzidis, Nanostructured Thermoelectrics: The New Paradigm?†, Chem. Mater. 22(3) (2010) 648-659.
[17] B.A. Cook, M.J. Kramer, J.L. Harringa, M.-K. Han, D.-Y. Chung, M.G. Kanatzidis, Analysis of Nanostructuring in High Figure-of-Merit Ag1-xPbmSbTe2+mThermoelectric Materials, Adv. Funct. Mater. 19(8) (2009) 1254-1259.
[18] I.-H. Jung, D.-H. Kang, W.-J. Park, N.J. Kim, S. Ahn, Thermodynamic modeling of the Mg–Si–Sn system, Calphad 31(2) (2007) 192-200.
[19] S. Muntyanu, E. Sokolov, E. Makarov, STUDY OF THE MG 2 SN-MG 2 SI SYSTEM, Izv Akad Nauk Ussr Neorgan Materialy 2(5) (1966) 870-875.
[20] E. Nikitin, E. Tkalenko, V. Zaitsev, A. Zaslavskii, A. Kuznetsov, A study of the phase diagram for the Mg2Si-Mg2Sn system and the properties of certain of its solid solutions, Inorg. Mater. 4 (1968) 1656-9.
[21] L. Chen, G. Jiang, Y. Chen, Z. Du, X. Zhao, T. Zhu, J. He, T.M. Tritt, Miscibility gap and thermoelectric properties of ecofriendly Mg2Si1−xSnx ($0.1 \leq x \leq 0.8$) solid solutions by flux method, J. Mater. Res. 26(24) (2011) 3038-3043.
[22] A. Sizov, H. Reardon, B.B. Iversen, P. Erhart, A.E. Palmqvist, Influence of Phase Separation and Spinodal Decomposition on Microstructure of Mg2Si1–x Sn x Alloys, Crystal Growth & Design 19(9) (2019) 4927-4933.
[23] S. Vivès, P. Bellanger, S. Gorsse, C. Wei, Q. Zhang, J.-C. Zhao, Combinatorial Approach Based on Interdiffusion Experiments for the Design of Thermoelectrics: Application to the Mg2(Si,Sn) Alloys, Chem. Mater. 26(15) (2014) 4334-4337.
[24] S. Gorsse, S. Vivès, P. Bellanger, D. Riou, L. Laversenne, S. Miraglia, D.R. Clarke, Multi-scale architectured thermoelectric materials in the Mg2(Si,Sn) system, Mater. Lett. 166 (2016) 140-144.
[25] C. Niu, C. Li, Z. Du, C. Guo, S. Chen, A thermodynamic assessment of the Bi–Mg–Sn ternary system, Calphad 39 (2012) 37-46.
[26] A.A. Kodentsov, G.F. Bastin, F.J.J. van Loo, The diffusion couple technique in phase diagram determination, J. Alloys Compd. 320(2) (2001) 207-217.
[27] J.S. Kirkaldy, Diffusion in Multicomponent Metallic Systems: Iii. The Motion of Planar Phase Interfaces, Can. J. Phys. 36(7) (1958) 917-925.
[28] H. Springer, A. Kostka, E. Payton, D. Raabe, A. Kaysser-Pyzalla, G. Eggeler, On the formation and growth of intermetallic phases during interdiffusion between low-carbon steel and aluminum alloys, Acta Mater. 59(4) (2011) 1586-1600.
[29] A. Baruah, M.K. Roy, S. Sarkar, N. Mandal, Dynamics of solid-melt front migration from a reaction–diffusion model, Heat Mass Transfer. 50(1) (2014) 31-38.
[30] R.M. German, Phase Diagrams in Liquid Phase Sintering Treatments, JOM 38(8) (1986) 26-29.
[31] H. Kamila, A. Sankhla, M. Yasseri, N.P. Hoang, N. Farahi, E. Mueller, J. de Boor, Synthesis of p-type Mg2Si1-xSnx with x = 0-1 and optimization of the synthesis parameters, Materials Today: Proceedings 8 (2019) 546-555.
[32] D. Kato, K. Iwasaki, M. Yoshino, T. Yamada, T. Nagasaki, Control of Mg content and carrier concentration via post annealing under different Mg partial pressures for Sb-doped Mg 2 Si thermoelectric material, J. Solid State Chem. 258 (2018) 93-98.

[33] M. Yasseri, N. Farahi, K. Kelm, E. Mueller, J. de Boor, Rapid determination of local composition in quasi-binary, inhomogeneous material systems from backscattered electron image contrast, Materialia 2 (2018) 98-103.
[34] J.-W. Liu, M. Song, M. Takeguchi, N. Tsujii, Y. Isoda, Transmission Electron Microscopy Study of Mg2Si0.5Sn0.5 Solid Solution for High-Performance Thermoelectrics, J. Electron. Mater. 44(1) (2015) 407-413.
[35] H. Gao, T. Zhu, X. Liu, L. Chen, X. Zhao, Flux synthesis and thermoelectric properties of eco-friendly Sb doped Mg 2 Si 0.5 Sn 0.5 solid solutions for energy harvesting, J. Mater. Chem. 21(16) (2011) 5933-5937.
[36] Y. Isoda, T. Nagai, H. Fujiu, Y. Imai, Y. Shinohara, Thermoelectric Properties of Sb-doped Mg2Si0.5Sn0.5, 2006 25th International Conference on Thermoelectrics, 2006, pp. 406-410.
[37] W. Gan, K. wu, M. Zheng, X. Wang, H. Chang, H.-G. Brokmeier, Microstructure and mechanical property of the ECAPed Mg 2Si/Mg composite, Materials Science and Engineering A-structural Materials Properties Microstructure and Processing - MATER SCI ENG A-STRUCT MATER 516 (2009) 283-289.
[38] J. de Boor, T. Dasgupta, H. Kolb, C. Compere, K. Kelm, E. Mueller, Microstructural effects on thermoelectric efficiency: A case study on magnesium silicide, Acta Mater. 77 (2014) 68-75.
[39] T. Dasgupta, C. Stiewe, J. de Boor, E. Müller, Influence of power factor enhancement on the thermoelectric figure of merit in Mg2Si0.4Sn0.6 based materials, physica status solidi (a) 211(6) (2014) 1250-1254.
[40] G. Borelius, Zur Theorie der Umwandlungen von metallischen Mischphasen. V Schwankungen und Kernbildung in unterkühlten Phasen, Annalen der Physik 425(6) (1938) 517-531.
[41] A. Hillert, Historic note on the two-peak miscibility gap, Journal of phase equilibria 15(1) (1994) 35-36.
[42] H. Okamoto, A two-peak miscibility gap, Journal of phase equilibria 14(3) (1993) 336-339.
[43] S.-i. Yi, V. Attari, M. Jeong, J. Jian, S. Xue, H. Wang, R. Arroyave, C. Yu, Strain-induced suppression of the miscibility gap in nanostructured Mg 2 Si–Mg 2 Sn solid solutions, Journal of Materials Chemistry A 6(36) (2018) 17559-17570.